Landslides (2019) 16:315–332
DOI 10.1007/s10346-018-1095-9
Received: 26 March 2018
Accepted: 24 October 2018
Published online: 7 November 2018

Gordon G. D. Zhou · Shuai Li · Dongri Song · Clarence E. Choi · Xiaoqing Chen

Depositional mechanisms and morphology of debris flow: physical modelling

Abstract A comprehensive understanding of the deposition mechanisms and morphology of debris flows is necessary to delineate the extent of a debris flow hazard. However, due to the wide range of debris flow compositions and the complex topography in the field, there remains a deficiency of fundamental understanding on how the effects of grain-size distribution, water content, and channel slope influence the deposition mechanisms and morphology of debris flow. In this study, a series of experimental tests were carried out using a flume with a horizontal outflow plane to discern the effects of particle size, water content, and slope on the deposition morphology and grain size segregation on the deposition fan. Results reveal that the experimental debris flows are under either viscous or collisional flow regimes. Most experimental debris flow fronts lack high pore fluid pressures, emphasizing the formation of deposits via grain-grain and grain-bed friction and collisions; also high excess pore fluid pressure (positive) behind the front head is measured and it is beneficial for the mobility of debris flows. Both the deposit area and runout-width ratio are positively correlated to the Bagnold and Savage numbers and the initial water contents. Furthermore, an increase of fines content reduces the runout distance. However, this feature is not as obvious for high water content flows ($w = 28.5\%$ in this study). Moreover, smoother transition topography between the transportation and deposition zone leads to longer runout distances. For debris flows with a high solid fraction ($C_s > 0.52$ in this study), particle sorting is quite inhibited in the deposit fan.

Keywords Debris flow · Flume model tests · Deposit morphology · Flow regimes · Grain size segregation

Introduction

Debris flows have been reported to cause devastating damage to infrastructure and even engulf entire towns (D'Agostino et al. 2010, 2013; Scheidl and Rickenmann 2010; Scheidl et al. 2013; Kim and Paik 2015; Chen and Cui 2017). Therefore, it is crucial to understand deposition mechanisms and morphology to enhance the mitigation of debris flows and to protect downstream facilities (cf. Major 1997; Iverson et al. 2010; Hürlimann et al. 2015; Shu et al. 2015).

Previous quantitative studies (e.g., Van Steun and Coutard 1989; Parsons et al. 2001; Dufresne 2012; Zhou et al. 2016) have been conducted to investigate the influence of sediment concentration, sediment size, water content, and slope on the runout distance of debris flows. Coincidentally, these investigations were carried in a uniform channel, which constrained lateral spreading and the extent to which the sediments were allowed to deposit naturally, thereby hindering the study of the morphology of the deposited sediments. In the field, natural debris flows exhibit different deposition morphologies (See Fig. 1: debris flows in Tsing Shan, Hong Kong in 1990 (Fig. 1a); Zhouqu, Gansu in 2010 (Fig. 1b); and Yingxiu, Sichuan in 2010 (Fig. 1c)). Clearly, findings from physical model tests in confined and uniform channels have less geomorphological relevance to the natural deposition fans that are generally observed in nature.

Haas et al. (2015) investigated debris flow fans using a 2-m-long flume model with a mean particle size of 0.5 mm. Findings showed that sediment composition is a key variable that influenced the runout distance, deposition area, levee height, lobe height, and lobe width of the deposited sediments. The term "sediment composition" refers to the particle size and concentration (Cui et al. 2017). Both of these variables control the mesoscopic grain shear stresses and determine whether grain-size segregation occurs (Johnson et al. 2012; Cui et al. 2018). Despite the importance of sediment composition, limited and systematic studies exist in literatures that examine how deposition mechanisms and morphology are governed by sediment composition.

Large-scale experiments have been conducted to demonstrate that debris flows tend to develop frictional and coarse-grained snouts, followed by a nearly liquefied and finer-grained body (Major and Iverson 1999; Iverson et al. 2010; Johnson et al. 2012). Although these studies have built a strong foundation for understanding deposition mechanisms, these experiments were carried out under very specific topographical conditions, which do not cover the entire spectrum of debris flow phenomenon observed around the world. For example, the accumulation of coarse clasts concentrating at the front head is usually unobvious in the highly viscous debris flows observed in Jiangjia Gully, China (Cui et al. 2005; Zhou and Ng 2010; Li et al. 2015). In such viscous flows, the particle-size distributions at the front and the tail of the flow are quite similar (cf. Cui et al. 2005; Zhou and Ng 2010). Clearly, researches focusing on a wider range of debris flow types and topography are beneficial in advancing the current state of understanding on debris flow deposition mechanisms and morphology.

In this study, a series of flume tests were carried out to discern the effects of water content, slope, and grain size distribution on the deposition mechanisms and morphology of the deposited sediments. Furthermore, the grain size segregation inside the post-depositional sediment is also interpreted to determine the deposit morphology.

Experimental method

Flume modelling

A flume model at the Dongchuan Debris Flow Observation and Research Station (DDFORS) of Chinese Academy of Sciences in Yunnan Province, China (N 26° 14′, E 103° 08′) was used for the experiments carried out in this study. The model has a rectangular channel with a width and depth of 0.30 and 0.35 m, respectively. The model has a storage tank at the most upstream end of the model. The storage tank has a maximum volume of 0.06 m^3 with a length of 1.0 m, depth of 0.8 m, and width of 0.3 m. The tank has a vertical gate to retain and release the debris material to simulate dam-break initiation. Downstream from the vertical gate are two channelized and inclinable sections. The channelized sections

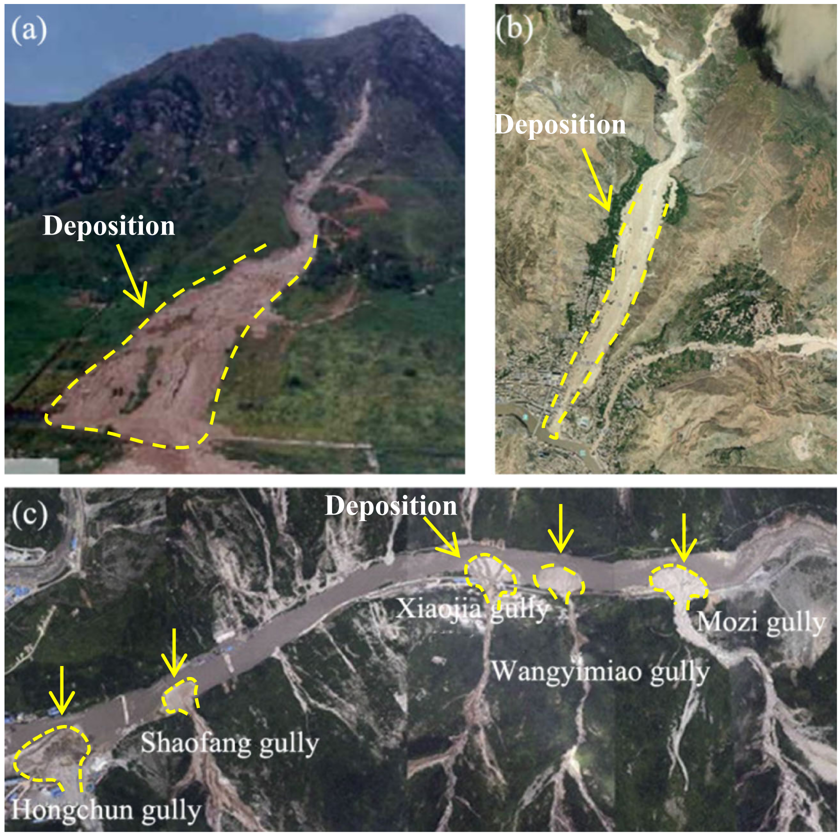

Fig. 1 Debris flow deposition. **a** Tsing Shan debris flow, 1990, Hong Kong (Sun et al. 2005). **b** Zhouqu debris flow, August 7, 2010, in Gansu Province of China (Cui et al. 2013). **c** Debris flow fans near Yingxiu town, August 14, 2010 (Tang et al. 2012). Arrows in the photographs show the deposition fans of debris flow events

transit into a horizontal outflow plane (Fig. 2) with length and width of 3.8 and 1.4 m, respectively. The base of the flume was constructed using steel plates, while the channel walls were constructed using glass. The two channelized sections inclined at different angles are herein referred to as the upstream channel (UC) and the downstream channel (DC). Two flume configurations were used in this study to investigate the effects of channel geometry on deposition mechanisms and morphology. In configuration I, UC is 3.0 m in length and is inclined at 45°, followed by the DC, which is 4.0 m in length and horizontal ($x = 0$ m is located at the connection point of UC and DC). Section DC transits onto the horizontal outflow plane, which is 3.8 m in length and 1.4 m in width. In the configuration II, UC is 3.0 m in length and inclined at 30°, followed by DC, which is 2.0 m in length and is inclined at 7.6°. Section DC transits onto the horizontal outflow plane.

Instrumentation
Two load cells were installed at the centerline position along the base of channel at an inclined distance of 2.0 m from the gate and 1.1 m downstream from the mouth of DC (Fig. 2) to measure the normal stress σ_{bed} of the debris flow. Above each pressure plate, the flow depth h of the debris was measured using a laser sensor (Leuze, ODSL 30/V-30M-S12) with a resolution of 1 mm. Also, pore pressure transducers (KPSI 735, 0~18 kPa) were installed to measure the pore pressure of the flow at the channel bed p_{bed}. Debris flow kinematics was captured using cameras (SONY FDR-AX40, 1440 × 1080 pixels, 25 fps) which were installed on crossbeams mounted over the channel.

Debris flow composition and experimental scheme
The sediments used for the debris flow mixtures are from the natural deposition fans of the Jiangjia Gully of the Xiaojiang Ravine near DDFORS. The grain-size distribution (GSD) of the sediments (> 0.25 mm) was measured by dry sieving. The fine content, particles passing the 0.25 mm sieve, was measured using a Malvern Mastersizer 2000, which is designed to measure the size of small particles or the distribution of different sizes within a sample, based on the laser diffraction principle and particle-size distribution statistics (Malvern Instruments Ltd., 2007). Two GSDs were investigated in this study. Figure 3 shows the two GSDs, herein referred to as GI and GII, which have median particle sizes (d_{50}) of 8.5 and 7.2 mm, respectively. The GSDs from Haas et al. (2015) and Iverson et al. (2010) are also shown for comparison. Note that the d_{50} in their debris flow mixtures are much smaller than that of this study.

In this study, four series of tests were carried out with sediments with two different grain-size distributions (i.e., GI and GII). The configuration of the flume was varied and referred to as configuration I (CI) and configuration II (CII). The mass of the sediments was kept constant while the water content was varied for each test, from 17.5 to 40% (equivalently to the volumetric solid fraction varied from 0.63 to 0.40). Due to the differences in the

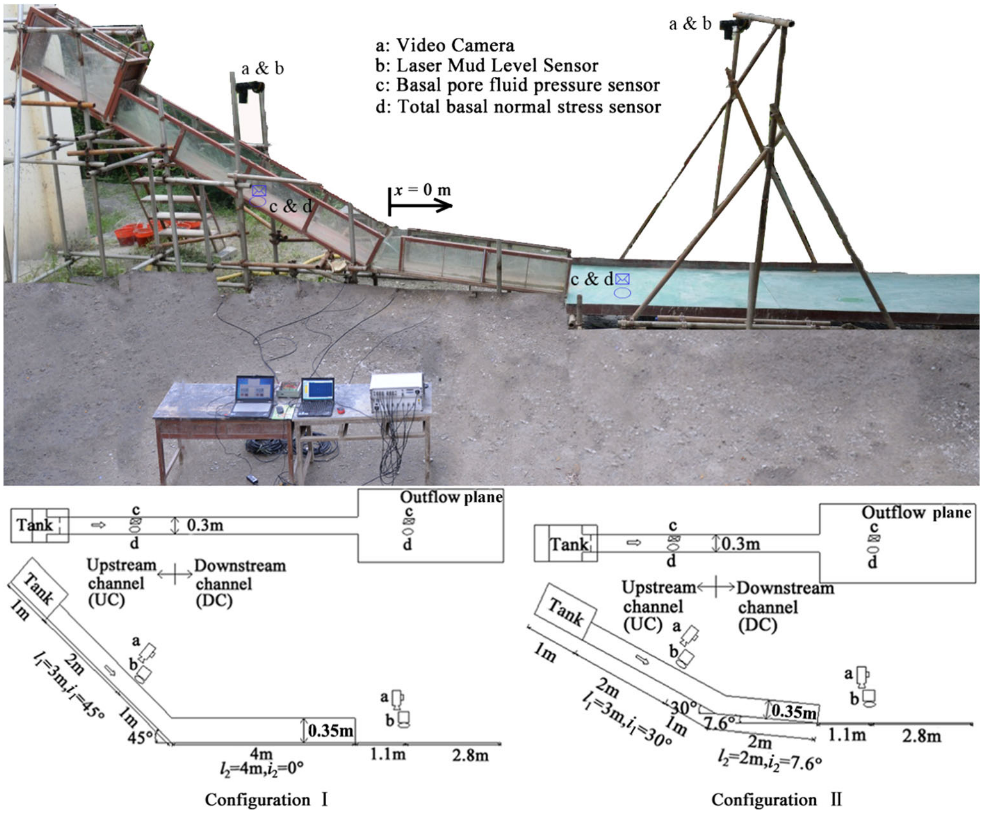

Fig. 2 Schematic diagram of the experimental flume setup

grain size distribution of the two soil samples, even with the same water content, there are slight differences in the bulk densities of the debris flows. By combination of different configuration and grain size distribution, effects of flume slope and grain size distribution could be comprehensively interpreted. The test program is summarized in Table 1.

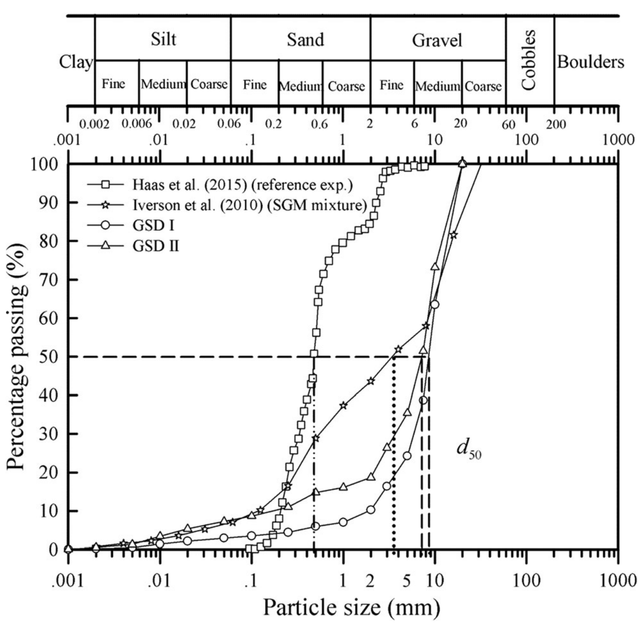

Fig. 3 Grain size distribution of the granular materials adopted in the modelling tests

Testing procedures

For each experiment, the gate was closed and a total volume of 0.03 m^3 of debris (mixture of sediments and water) was prepared in the tank. Then, the gate was immediately lifted to allow the debris flow to discharge downslope. Each experiment was conducted at least twice to ensure repeatability. The largest difference in the runout distance between any two tests was only 4.0%. Debris flow processes were photographed and recorded by using multiple cameras, and the videotape images were imprinted by using a high-precision timer synchronized with the data-acquisition system. After each test, the deposited debris was systematically sampled to investigate the spatial variation and distribution of different grain sizes. Sieving analysis was also carried out to measure the dry mass in nine one-ϕ bins, i.e., (1) < 0.25 mm, (2) 0.25–0.5 mm, (3) 0.5–1 mm, (4) 1–2 mm, (5) 2–3 mm, (6) 3–5 mm, (7) 5–7.5 mm, (8) 7.5–10 mm, and (9) 10–20 mm.

Dimensionless numbers and flow characterization

The Froude number *Fr* governs the dynamics of channelized debris flows (cf. Hübl et al. 2009; Iverson 1997, 2015). The *Fr* is the ratio of inertial to gravitational forces (Choi et al. 2015) and is given as follows:

$$Fr = \frac{v}{\sqrt{gh\cos\theta}} \qquad (1)$$

Table 1 Experimental test program

Test ID	Water content w (%)	Density ($\times 10^3$ kg/m^3)	Solid fraction C_s	Froude number Fr	Bagnold number N_{Bag}	Savage number N_{Sav}	Friction number N_{Fric}
CI-GI-17.5	17.5	2.199	0.63	3.0	71.43	1.12	63.81
CI-GI-19.0	19.0	2.123	0.61	3.2	77.02	1.42	54.18
CI-GI-20.0	20.0	2.119	0.60	3.3	89.31	1.60	55.75
CI-GI-23.0	23.0	2.106	0.57	3.5	91.35	1.88	48.68
CI-GII-17.5	17.5	2.183	0.57	3.2	46.15	1.29	35.69
CI-GII-19.0	19.0	2.128	0.55	3.3	45.50	1.37	33.21
CI-GII-20.0	20.0	2.118	0.54	3.4	52.47	1.49	35.14
CI-GII-21.5	21.5	2.059	0.53	3.3	60.91	1.44	42.18
CI-GII-23.0	23.0	2.044	0.51	3.5	64.14	1.70	37.63
CI-GII-24.5	24.5	2.026	0.50	3.4	62.34	1.66	37.52
CI-GII-26.5	26.5	1.965	0.49	3.8	84.52	2.36	35.79
CI-GII-28.5	28.5	1.912	0.47	4.2	107.32	3.40	31.61
CI-GII-30.0	30.0	1.875	0.46	4.7	138.47	4.40	31.45
CII-GII-22.0	22.0	2.056	0.52	3.8	72.67	2.45	29.68
CII-GII-24.5	24.5	2.026	0.50	4.0	72.73	2.20	33.08
CII-GII-26.5	26.5	1.965	0.49	4.0	82.56	1.85	44.65
CII-GII-28.5	28.5	1.912	0.47	4.1	92.10	1.97	46.67
CII-GII-30.0	30.0	1.875	0.46	4.8	135.53	3.82	35.46
CII-GII-32.5	32.5	1.851	0.44	5.2	181.09	6.28	28.82
CII-GII-35.0	35.0	1.820	0.43	5.9	269.31	9.03	29.82
CII-GII-40.0	40.0	1.736	0.40	6.6	313.82	12.21	25.71
CII-G I-28.5	28.5	1.975	0.52	3.2	114.02	2.48	46.02

Test ID "CI-GI-17.5" represents "Configuration I, GSD I, Water content $w = 17.5\%$"

where v is velocity, g is the acceleration due to earth's gravity, h is the approaching flow depth, and θ is the channel inclination. In this study, the measured Fr ranges from 3.0 to 6.6 (see Table 1), which falls the range of flow dynamics of geophysical flows that engineers generally mitigate ($0.1 < Fr < 10$) (Faug 2015).

There are three important stresses that govern the motion of a debris flow, specifically inertial, frictional, and viscous stresses (Iverson 1997; Iverson and Denlinger 2001; Parsons et al. 2001; Hsu et al. 2008; Zhou and Ng 2010). Inertial forces arise from short-term collisions between solid grains, frictional forces are associated to enduring contacts between grains, and viscous forces are controlled by viscosity of the pore fluid (slurry) and relative shearing between the solid and fluid phases (Stancanelli et al. 2015). The relative importance and dominance between these forces are characterized by the Bagnold number N_{Bag}, Savage number N_{Sav}, and Friction number N_{Fric}. The N_{Bag} defines the ratio of inertial to viscous forces and is given as follows:

$$N_{Bag} = \frac{C_s \rho_s \delta^2 \dot{\gamma}}{(1-C_s)\mu} \tag{2}$$

where δ is the characteristic grain size of the sediments in the debris flow, ρ_s is density of the solids (2750 kg/m^3 at DDFORS, Zhou and Ng 2010), μ is the interstitial fluid viscosity, C_s is the volumetric solid fraction, and $\dot{\gamma}$ is the shear rate and it can be approximately estimated by:

Table 2 Comparison of key dimensionless numbers

Dimensionless number	Small-scale flume (this study)	Small-scale flume (Haas et al. 2015)	USGS flume (Iverson 1997)	Recorded natural debris flows (Haas et al. 2015)
N_{Bag}	45–314	37–1589	400	$1–10^8$
N_{Sav}	0.5–9.0	0.17–2.25	0.20	$10^{-7}–1$
N_{Fric}	25–64	141–2760	2000	$1–10^5$

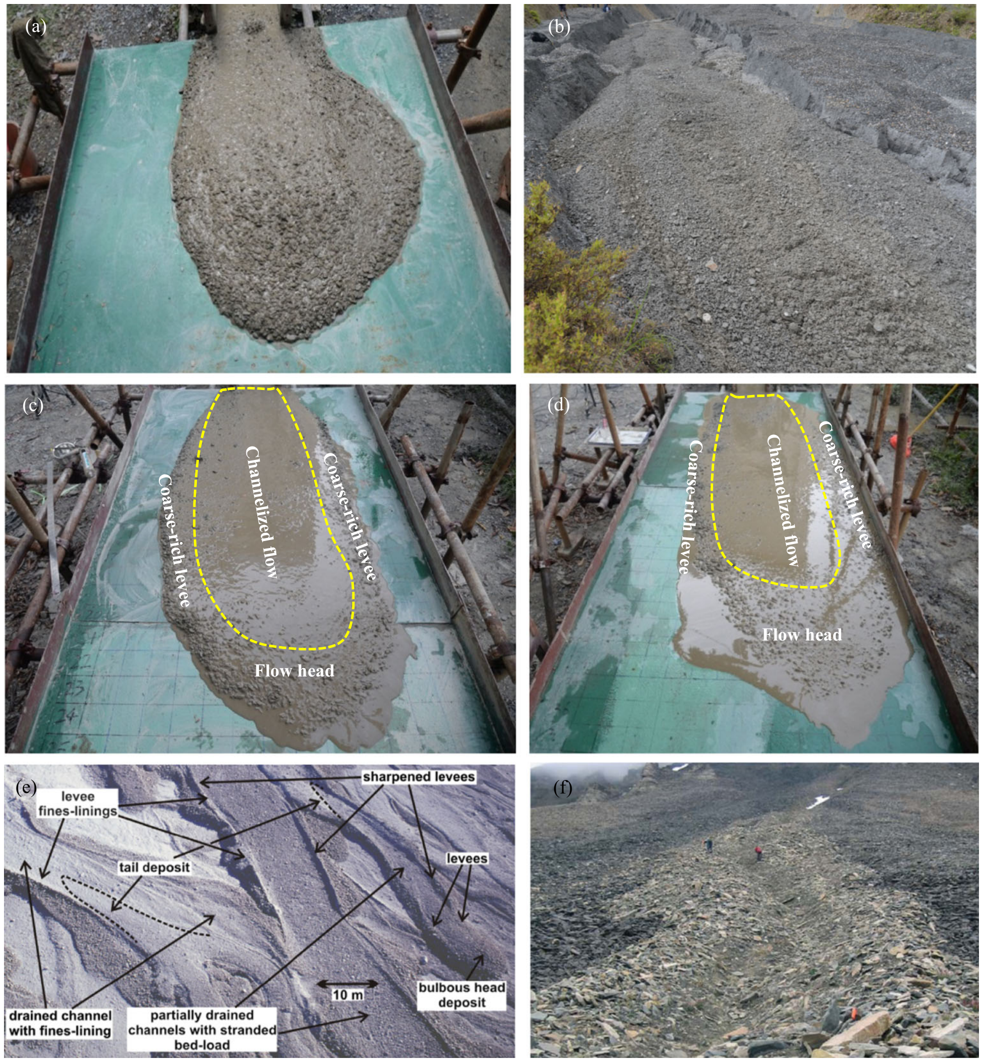

Fig. 4 Morphological features observed in the debris flow deposition. **a** CII-GII-22.0 ($w = 22.0\%$; $C_s = 0.52$). **b** A natural debris flow event in Jiangjia Gully. **c** CII-GII-26.5 ($w = 26.5\%$; $C_s = 0.49$). **d** CII-GII-35.0 ($w = 35.0\%$; $C_s = 0.43$). **e** Pumiceous pyroclastic flow deposits at Mount St Helens, USA (cf. Kokelaar et al. 2014). **f** Coarse-grained levees in natural debris flows on Svalbard (cf. Haas et al. 2015)

$$\dot{\gamma} = \frac{v}{h} \tag{3}$$

The N_{Sav} is the ratio of grain-inertial-to-contact frictional forces and is given as follows:

$$N_{\mathrm{Sav}} = \frac{\rho_s \delta^2 \dot{\gamma}^2}{\left(\rho_s - \rho_f\right) g h \tan\phi} \tag{4}$$

where ϕ is the friction angle between grains (30° for the granular materials at DDFORS, Zhou and Ng 2010) and ρ_f is the density of the fluid (assumed to be 1000 kg/m^3).

The ratio of grain-contact to fluid viscous stresses is defined as the Friction number, N_{Fric}, which is given as follows:

$$N_{\mathrm{Fric}} = \frac{C_s\left(\rho_s - \rho_f\right) g h \tan\phi}{(1 - C_s)\dot{\gamma}\mu} \tag{5}$$

These dimensionless numbers enable comparisons of the relative importance of the aforementioned stresses at different scales and link experimental observations with physical stresses (Zhou and Ng 2010; Haas et al. 2015; Iverson 2015). A summary of the comparison of dimensionless numbers from this study, small-scale tests (Haas et al. 2015), large-scale tests, and natural flows (Iverson 1997) is given in Table 2.

Interpretation of test results

Deposit morphology, stress level, and flow regimes of debris flow

Morphology of deposited sediments

Typically, as a debris flow accelerates down a channel, a flow front that is rich in coarse grains develops via particle-size segregation

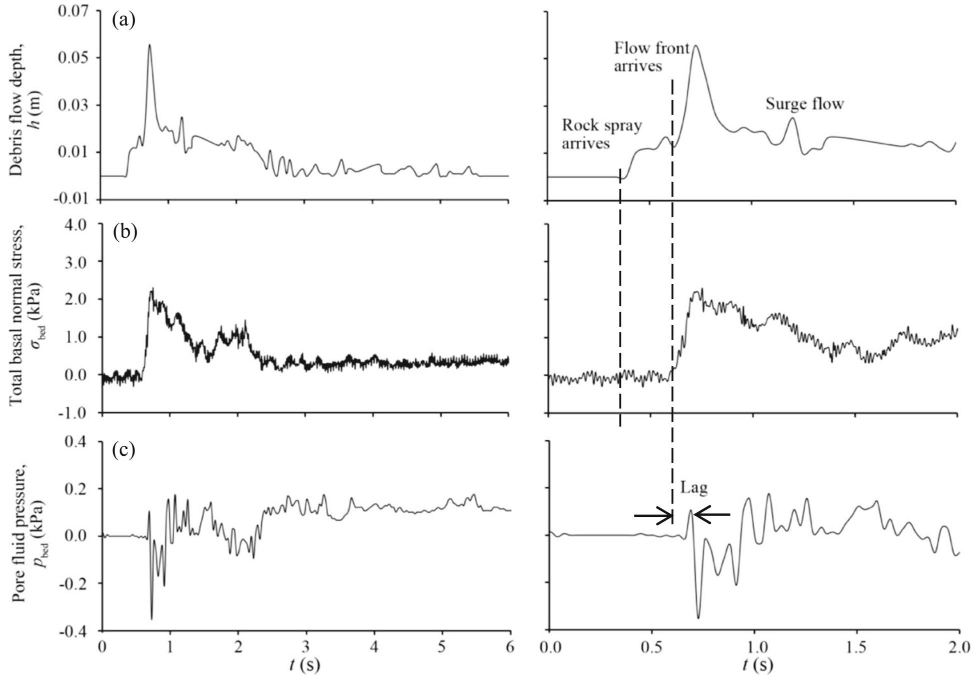

Fig. 5 Representative measurements of **a** debris flow depth, **b** total basal normal stress, and **c** basal pore fluid pressure along UC 2.0 m downslope of the gate for test CII-GII-24.5. Full time-history shown on left; magnified time-history on right

(Johnson et al. 2012). The coarse-grained-front is followed by a saturated body comprising finer grains. The advancing flow head is thicker than both the body and tail of the flow. Sediment deposits near the head of the flow eventually lose momentum and the sediments are shoveled aside by the trailing debris to form lateral levees, which provide a natural confinement for the flow. The lateral levees are steepest where the coarsest granular material deposits. The deposition process occurs in transient surges. The flow kinetic energy is dissipated via longitudinally and laterally spreading.

Figure 4 shows a comparison of the morphological features of the deposition profiles resulting from flume configuration CII and GSD II. The water content is varied from 22.0 to 35.0%. Significant differences among experimental subsets are observed in the

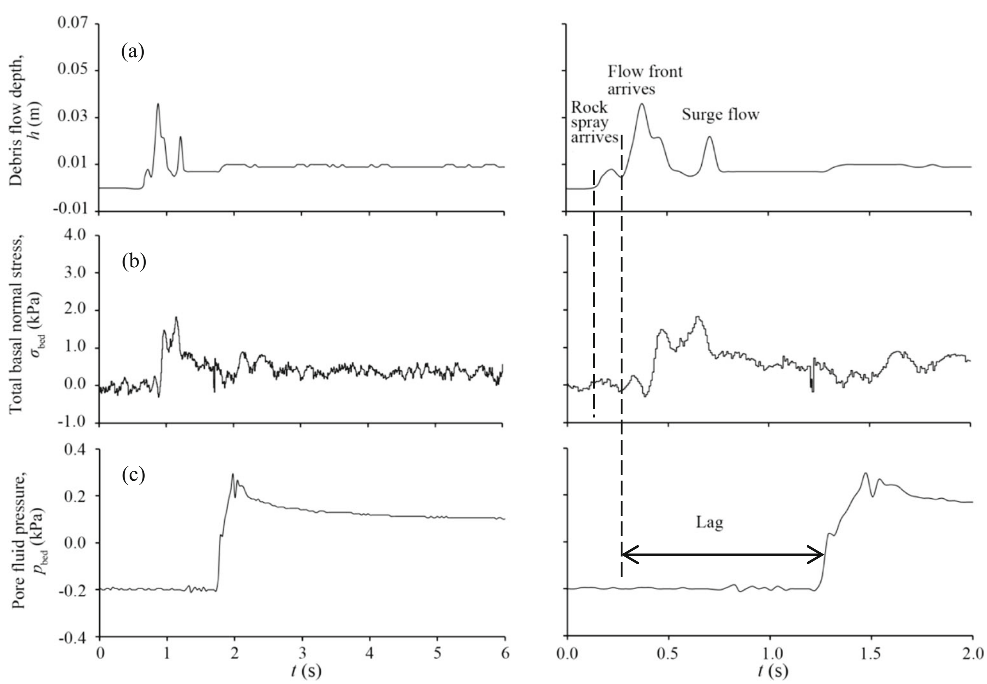

Fig. 6 Representative measurements of **a** debris flow depth, **b** total basal normal stress, and **c** basal pore fluid pressure in the runout area1.1 m beyond the flume mouth for test CII-GII-24.5. Full time-history shown on left; magnified time-history on right

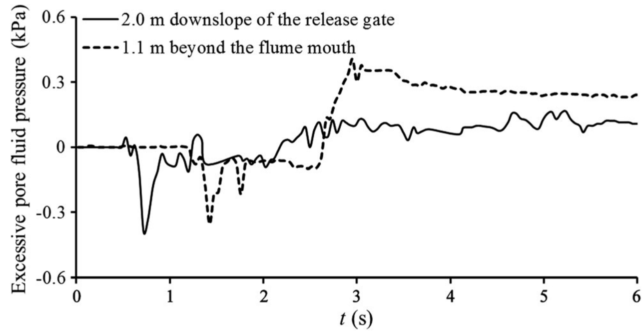

Fig. 7 Time-evolution of the excessive pore fluid pressure at the flume bed and outflow plain

deposited morphology. For the debris mixture with the lowest water content (Fig. 4a), the mobility is the least among the other tests. Also, lateral levees are less obvious and less particle-size segregation occurred in this debris flow. Similar phenomenon is observed in the deposits of a natural debris flow in Jiangjia Gully (Fig. 4b). By contrast, lateral levees are more obvious for the mixtures with higher water content (Fig. 4c, d). The heads of the flows with higher water content are driven further along the outflow plane within the confines of the lateral levees. The advancing flow head and lateral levees are thicker than the central channels. The deposits exhibited morphologic features resembling a natural pyroclastic flow deposits at Mount St Helens, USA

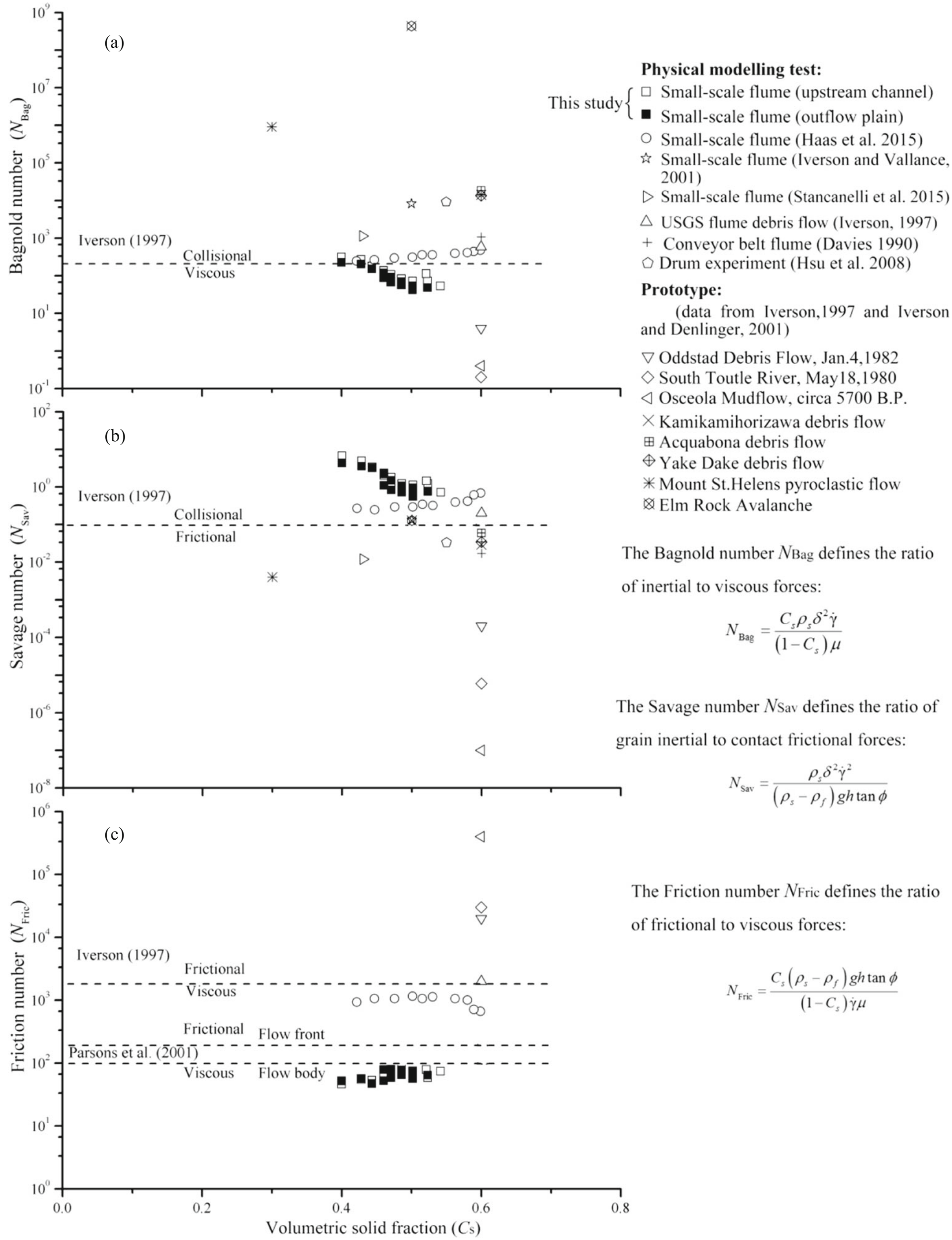

Fig. 8 The flow regimes observed in this study and those from previous researches. **a** Bagnold number versus solid fraction. **b** Savage number versus solid fraction. **c** Friction number versus solid fraction

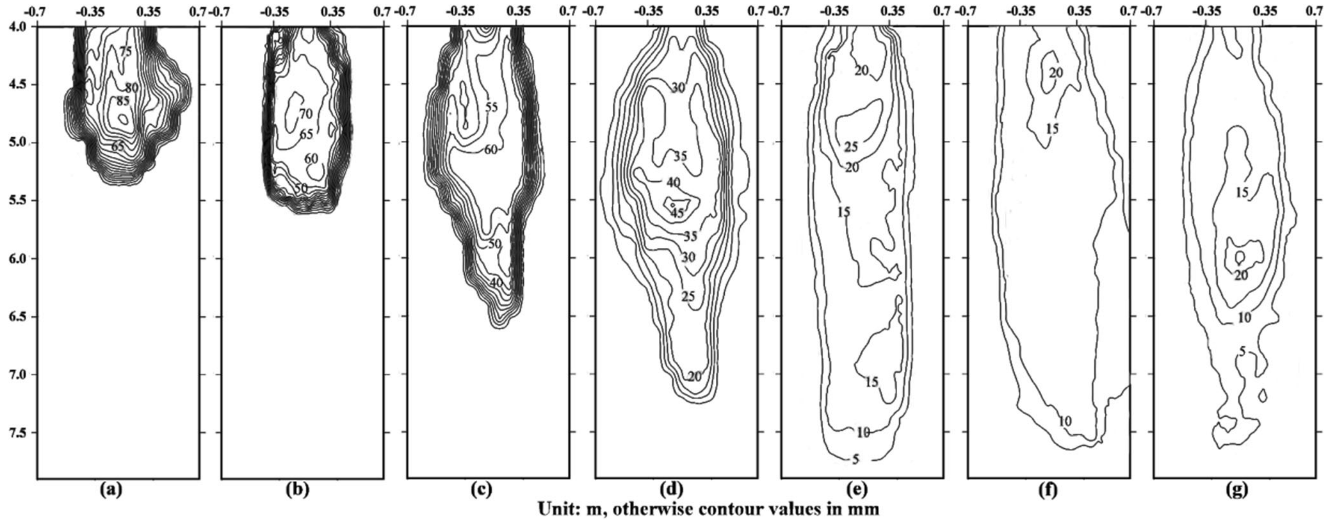

Fig. 9 Influence of water content on deposition morphology (CII-GII). **a** $w = 22.0\%$ ($C_s = 0.52$). **b** $w = 24.5\%$ ($C_s = 0.50$). **c** $w = 26.5\%$ ($C_s = 0.49$). **d** $w = 28.5\%$ ($C_s = 0.47$). **e** $w = 32.5\%$ ($C_s = 0.44$). **f** $w = 35.0\%$ ($C_s = 0.43$). **g** $w = 40.0\%$ ($C_s = 0.40$)

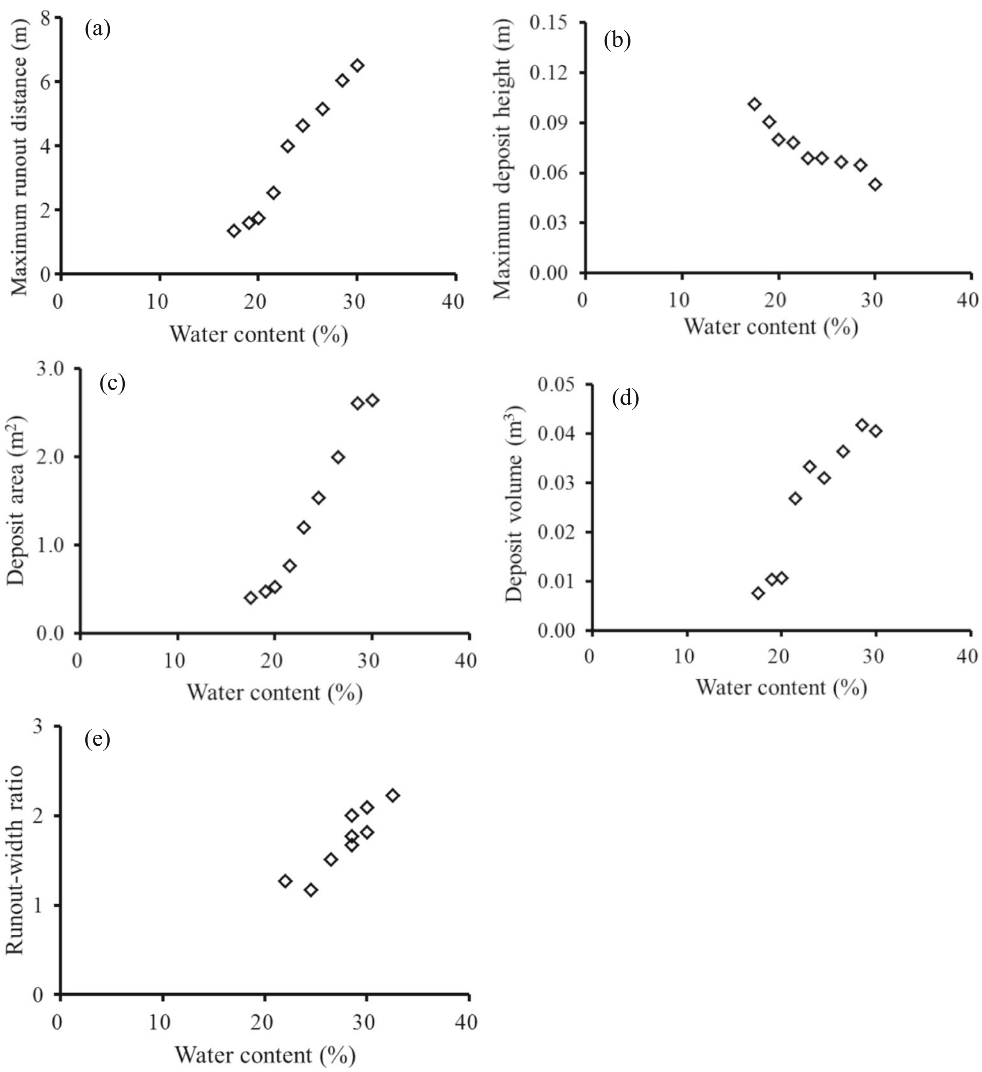

Fig. 10 Relationship between debris flow water contents and **a** runout distance, **b** maximum deposit height, **c** deposit area, **d** deposit volume, and **e** runout-width ratio

(Fig. 4e) and a natural debris flow at Svalbard (Fig. 4f) such as lobate shapes, steep, and blunt margins.

Stress level during debris flow deposition process

Figures 5 and 6 show the typical measurements (test CII-GII-24.5) from a load cell installed at the base of UC and the outflow plane, respectively. Flow depth (Figs. 5a and 6a), normal stress (Figs. 5b and 6b), and pore pressure (Figs. 5c and 6c) measurements were measured simultaneously to characterize debris flow motion and deposition. The time is 0 s when the debris mixture is released from the storage tank.

Basal total normal stress almost increases proportionately with flow depth, except for a few brief intervals at the UC (Fig. 5) and the outflow plane (Fig. 6). Multiple surges develop behind the flow front and are reflected in the time-histories. Changes in amplitude and position of the waves (with respect to the flow front) are causing temporal variations in the rapid moving of debris flow surges.

The basal normal stresses rapidly increase, whereas the pore fluid pressure remained almost null at the flow front and rapidly increased after the flow front has passed (Figs. 5c and 6c). A time lag is observed between the abrupt changes of bed-normal stress and the abrupt rise in basal pore fluid pressure of less than 0.1 s at UC (Fig. 5c) and about 1.0 s at the outflow plane (Fig. 6c). This delay implies that the flow front is composed of relatively dry coarse grains with high permeability and that rapidly diffuses pore pressure. A longer time lag at the outflow plane reflects the flow front lacking positive pore fluid pressure lasts longer distance during the deceleration and deposition process. These measurements further corroborate that the mechanisms of debris flow deceleration through enhanced shear stresses (Zhou et al. 2018) and flow energy dissipation via grain-grain and grain-bed friction and collision (Johnson et al. 2012) due to the presence of an unsaturated front. Additionally, it is worthwhile to note that the pore fluid pressure lasts longer than the period for data sampling. This shows the low permeability of the quasi-statically consolidating debris material. Results from this study are consistent with field observation of natural debris flows: the head is relatively dry, whereas the trailing debris is saturated with slurry and remains liquefied (cf. Hürlimann et al. 2003; McArdell et al. 2007).

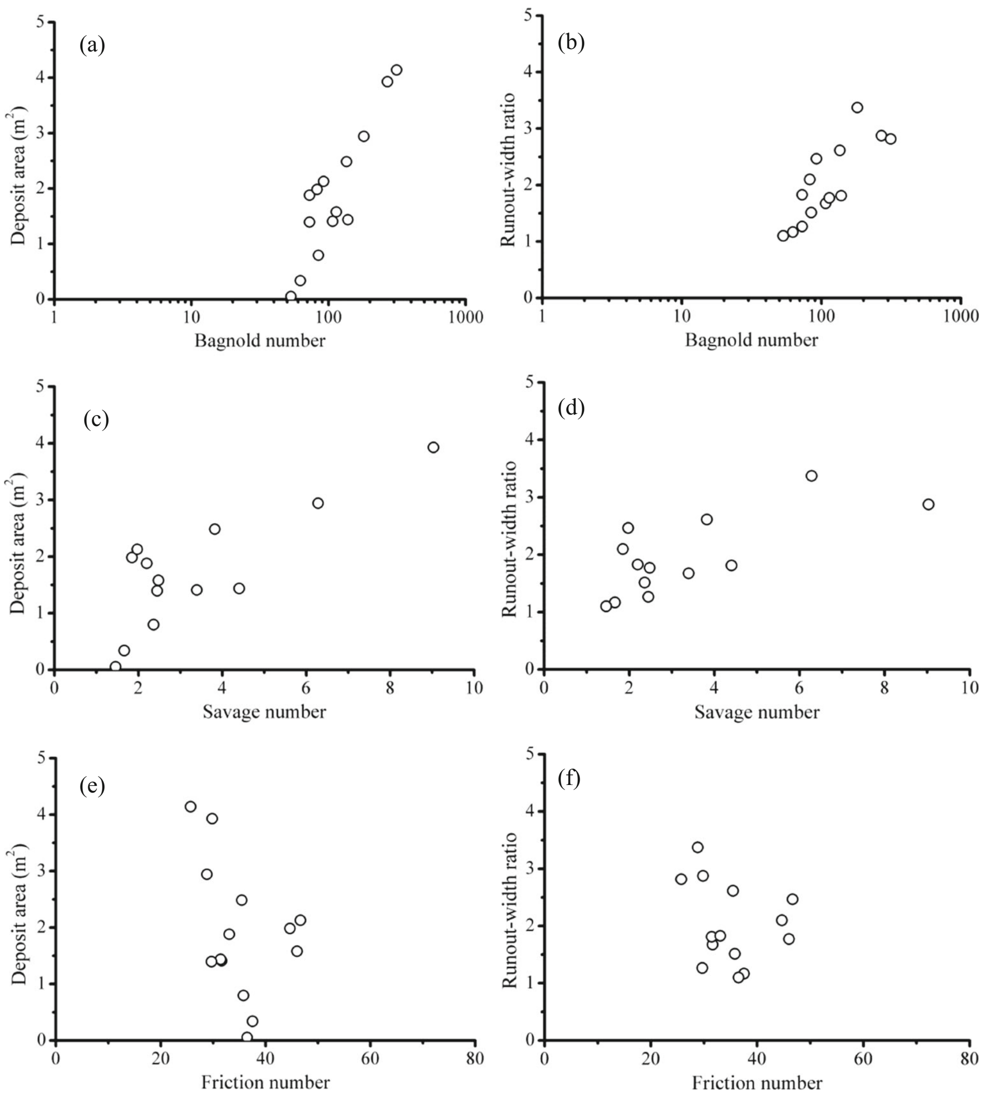

Fig. 11 Relationship between deposit area, runout-width ratio, and the Bagnold number (**a** and **b**), Savage number (**c** and **d**), and Friction number (**e** and **f**)

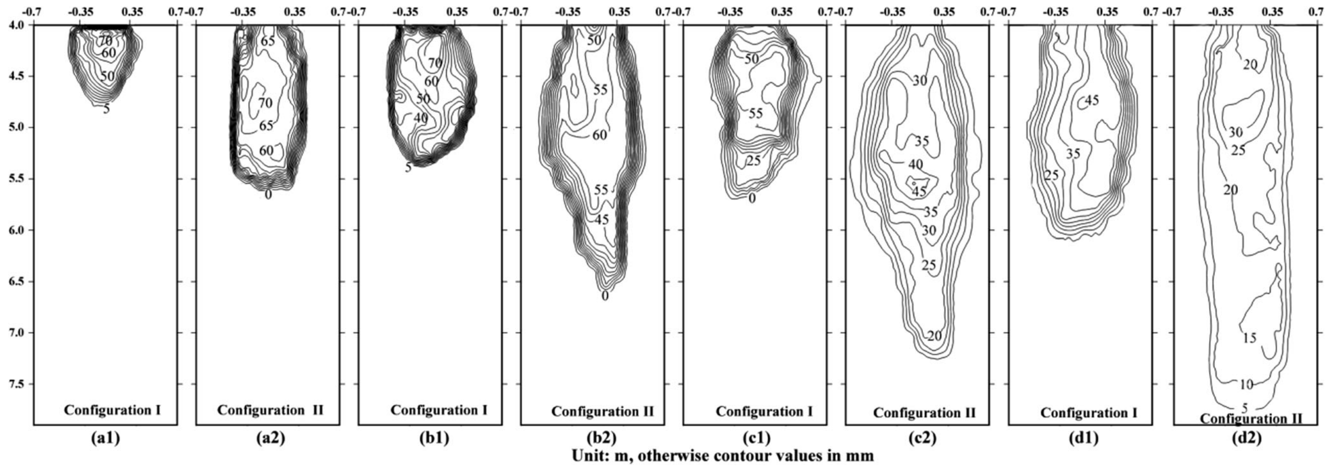

Fig. 12 Effects of slope on morphology of deposited debris (CI-GII and CII-GII). $w = 24.5\%$: (a1) and (a2); $w = 26.5\%$: (b1) and (b2); $w = 28.5\%$: (c1) and (c2); $w = 30.0\%$: (d1) and (d2)

The time-history of excessive pore fluid pressure Δu is calculated as follows:

$$\Delta u = p_{\text{bed}} - \rho_f g h \tag{6}$$

Figure 7 indicates that the excessive pore fluid pressure decreases abruptly when the flow front passes the point of measurement and persists even after debris flow deposition. This observation is consistent with previous results presented by Iverson (1997), Iverson and Vallance (2001), and Major and Iverson (1999) in their large-scale flume experiments. Excessive pore fluid pressures persist in debris flow interiors without sufficient time to dissipate, which in turn influences the grain stresses in the core of a debris flow. These results further corroborate the

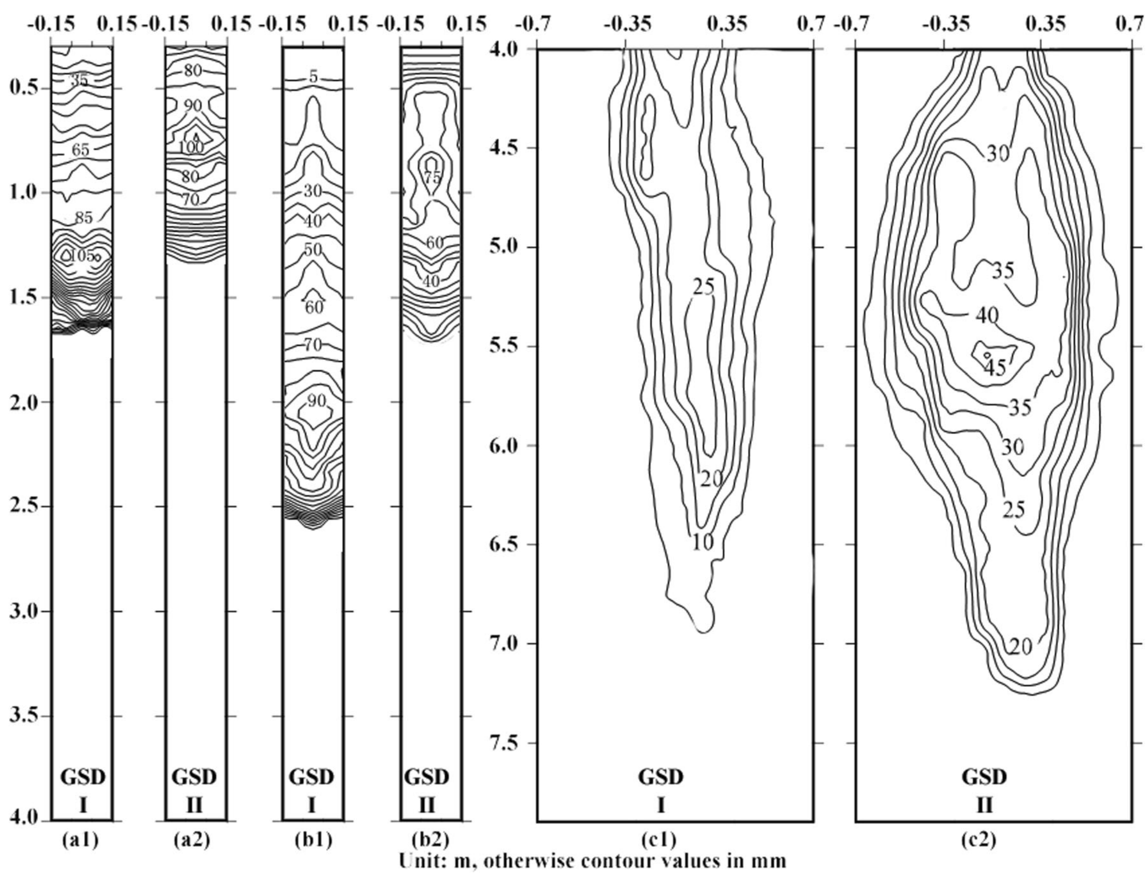

Fig. 13 Morphological properties as an effect of the GSD. The flow front stopped at the DC when $w < 23.0\%$ ($C_s > 0.51$); (a1) and (a2): $w = 17.5\%$; (b1) and (b2): $w = 20.0\%$. The debris flow beyond the flume mouth and deposit at the outflow plan when $w > 23.0\%$ ($C_s < 0.51$); (c1) and (c2): $w = 28.5\%$

idea that sustained excessive pore fluid pressures contribute to their unusual mobility.

Flow regimes of debris flow deposition process

Figure 8 shows a comparison of the test results from this study with the model flows from small-scale flume tests (Haas et al. 2015; Stancanelli et al. 2015), large-scale flume model tests (Iverson 1997), conveyor belt flume tests (Davies 1990), drum experiments (Hsu et al. 2008), and natural debris flows (Hsu 1975, 1978; Kuntz et al. 1981; Wilson and Head 1981; Hoblitt 1986; Takahashi 1991; Berti et al. 1999, 2000).

The Bagnold numbers, N_{Bag}, of the flows in this study are similar in magnitude compared to that of the flows that developed in the large-scale flume tests and natural debris flows (Fig. 8a), while the N_{Sav} is systematically higher (Fig. 8b) and the N_{Fric} is systematically lower (Fig. 8c) than the reported large-scale and natural flows. The differences in the observed magnitudes are because the flows developed in this study exhibit higher shear rates and higher fluid viscosity due to the high fines content from the natural sediments obtained from the Jiangjia Gully. Furthermore, results show that both N_{Bag} and N_{Sav} decrease with higher solid fractions (Fig. 8a, b). This implies that a higher solid fraction

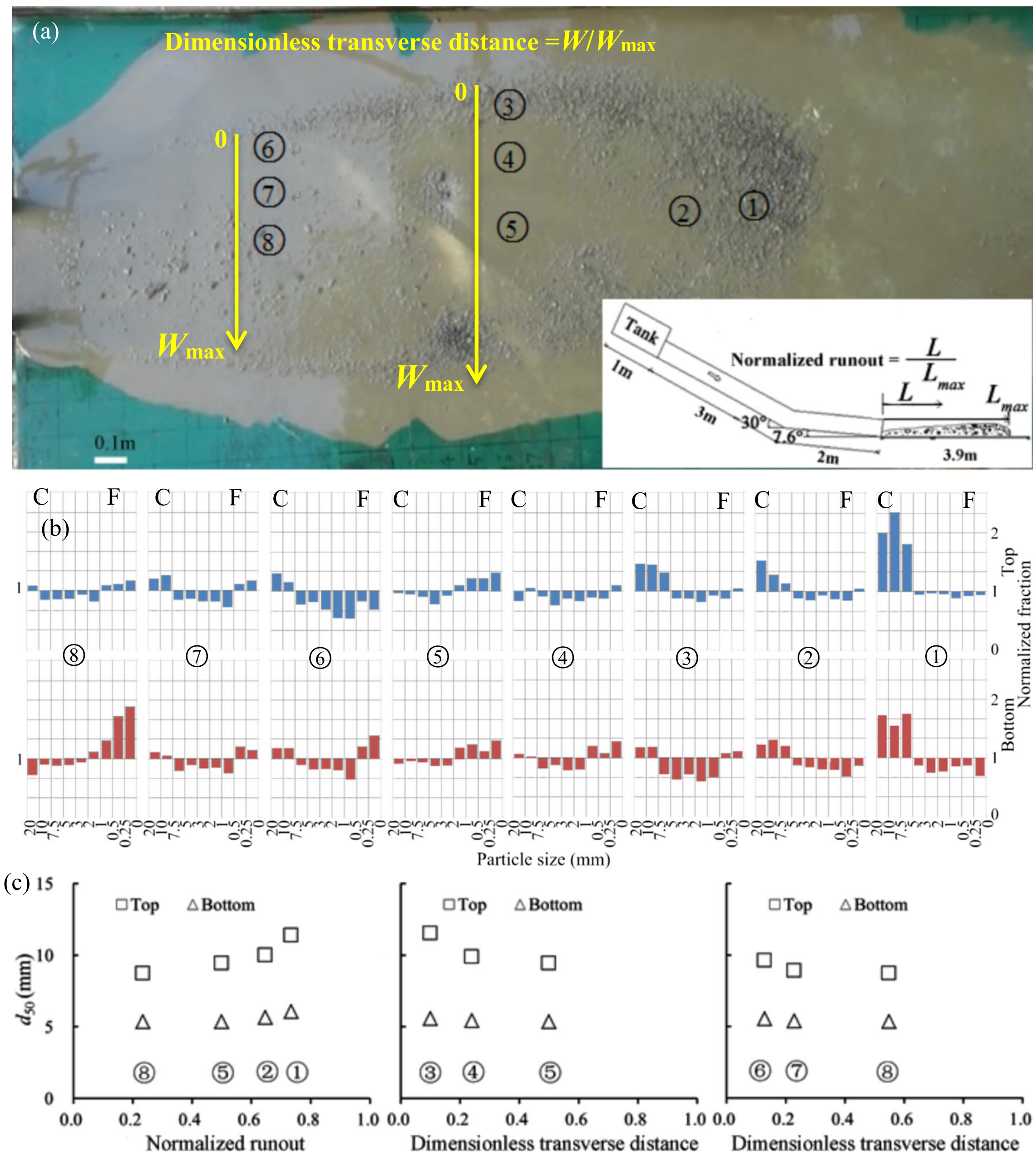

Fig. 14 Deposition and sample sites **a** in the fan of experimental debris flow with $w = 40.0\%$ ($C_s = 0.40$). **b** Relative abundance plots of deposit granulometry of samples. Coarse material (C) is to the left and fine material (F) to the right. Bars below the centerline indicate depletion and those above the centerline indicate enrichment. **c** The mean particle size (d_{50}) of each sample

in a flow diminishes the effects of viscous drag and grain-inertial stresses. Similarly, higher solid fractions lead to higher Friction number (Fig. 8c), which suggests more pronounced enduring grain-contact stresses relative to viscous stresses. Surprisingly, the results presented by Haas et al. (2015) show different correlations compared to the findings in this study, particularly in the changes of Bagnold numbers and Savage numbers (Fig. 8a, b). Differences are likely due the composition of the debris material used in present experiments and Haas et al. (2015). Furthermore, the channel lengths are quite different. Compared with the length of the flume (5.0–7.0 m) used in this study, the flume used by Haas et al. (2015) is only 2 m in length. The flume length influences the extent to which a debris flow develops. More importantly, the particle sizes adopted by Haas et al. (2015) are much smaller than those used in this study. The differences in particle size can lead to changes in grain-inertial forces (the solid inertial stress, $T_{s(i)} \sim C_s \rho_s \delta^2 \dot{\gamma}^2$, cf. Zhou and Ng 2010).

Experimental data shows that the debris flows in this study transition from collisional dominated flows to viscous dominated flows with an increasing solid fraction. This observed phenomenon coincides with that reported by Iverson (1997), whereby collisional stresses dominate over viscous and frictional stresses when $N_{Bag} > 200$ and $N_{Sav} > 0.1$, respectively. Notwithstanding, there exists two ideologies on the thresholds that characterize the transition between frictional and

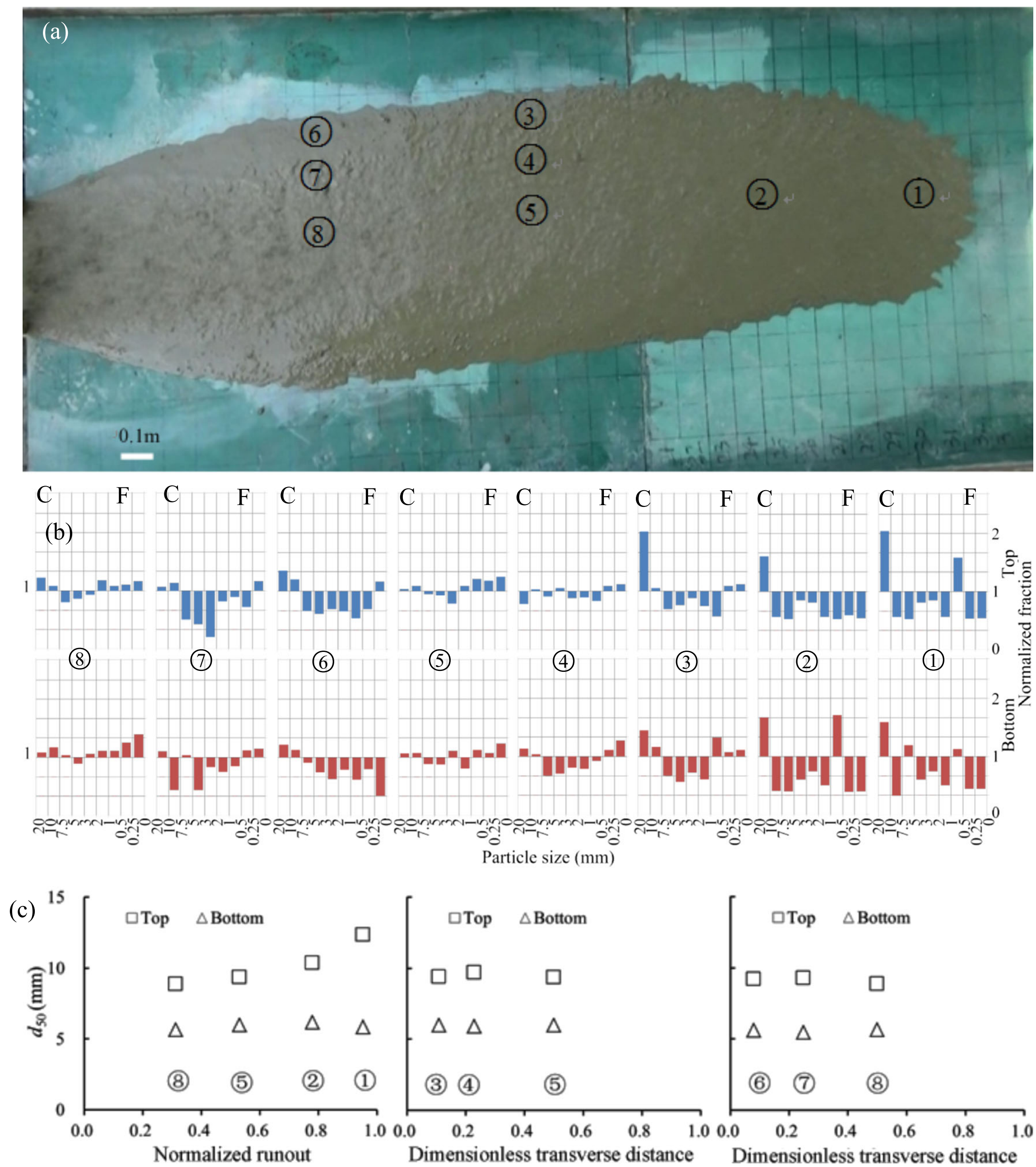

Fig. 15 Deposition and samples sites **a** in the fan of experimental debris flow with $w = 32.5\%$ ($C_s = 0.44$). **b** Relative abundance plots of deposit granulometry of samples. Coarse material (C) is to the left and fine material (F) to the right. Bars below the centerline indicate depletion and those above the centerline indicate enrichment. **c** The mean particle size (d_{50}) of each sample

viscous flow regimes. More specifically, Iverson (1997) reported $N_{Fric}>2000$ for debris flows, and Parsons et al. (2001) reported $N_{Fric}>100$ for the flow body and $N_{Fric}>250$ for the flow front based on sediment-water mixture flow experiments. Different threshold values suggest that changes among collisional, frictional, and viscous regimes depend strongly on the flow composition.

Results from this study suggest that a wide range of natural debris flows exists and results using one type of flow composition cannot be universally applicable to the dynamics of all types of debris flows. The flow regimes of the present research indicate that the dynamics of debris flows are predominantly governed by grain-contact and fluid viscous drag forces. The flow front can be characterized as grain-contact dominated with an increasing interface friction angle as deposition progresses. Furthermore, results indicate that the deposition processes of most debris flows in this study are mainly affected by grain-inertial stresses. For model flows within the viscous regime, the deposition processes may be governed by high fluid viscosity due to increased yield strength of slurries (mixtures of fines and water).

Key influence factors on debris flow deposit morphology

Effects of water content

A series of experimental tests (No. CII-GII-22.0 to No. CII-GII-40.0 in Table 1) was conducted to discern the effects of water content on

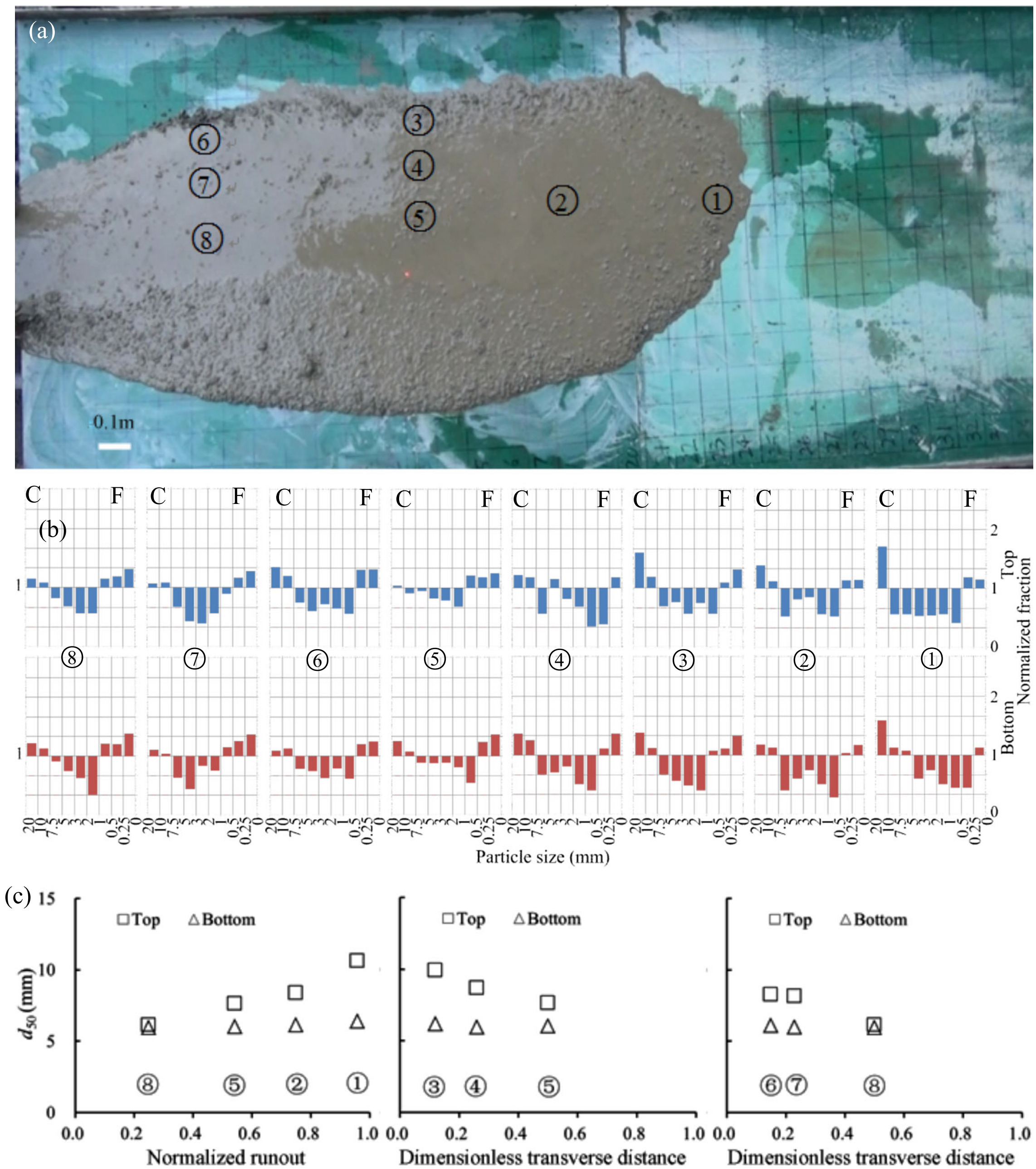

Fig. 16 Deposition and samples sites (**a**) in the fan of experimental debris flow with $w=26.5\%$ ($C_s=0.49$). **b** Relative abundance plots of deposit granulometry of samples. Coarse material (C) is to the left and fine material (F) to the right. Bars below the centerline indicate depletion and those above the centerline indicate enrichment. **c** The mean particle size (d_{50}) of each sample

the morphology of deposited material. Results show that debris flows with water contents lower than 22.0% are not very mobile and are unable to run out to the end of DC. Figure 9a shows the model flow with a water content $w = 22.0\%$ (solid fraction $C_s = 0.52$). The deposition area of the debris is the smallest and the runout length is also the shortest compared to other tests. The morphology exhibits an oval shape and has the greatest thickness. As the water content increases, progressive changes in morphology are observed (Fig. 9). More specifically, the morphology of the deposited material transitions towards longer and thinner lobes. In essence, higher water contents lead to longer, thinner, and shallower deposits. This observation is because of higher water content decrease grain-contact friction and bed friction resistance, thereby leading to more mobile flows.

Figure 10 shows the relationships among the water content, maximum runout distance, maximum deposit height, deposit area, deposit volume, and runout-width ratio. Results show a positive correlation between the water content and the maximum runout distance, deposit area, deposit volume, and runout-width ratio. By contrast, a negative correlation was observed between water content and the maximum deposition height. Debris flow runout and deposition height are highly sensitive to changes in water content. An increase of water content from

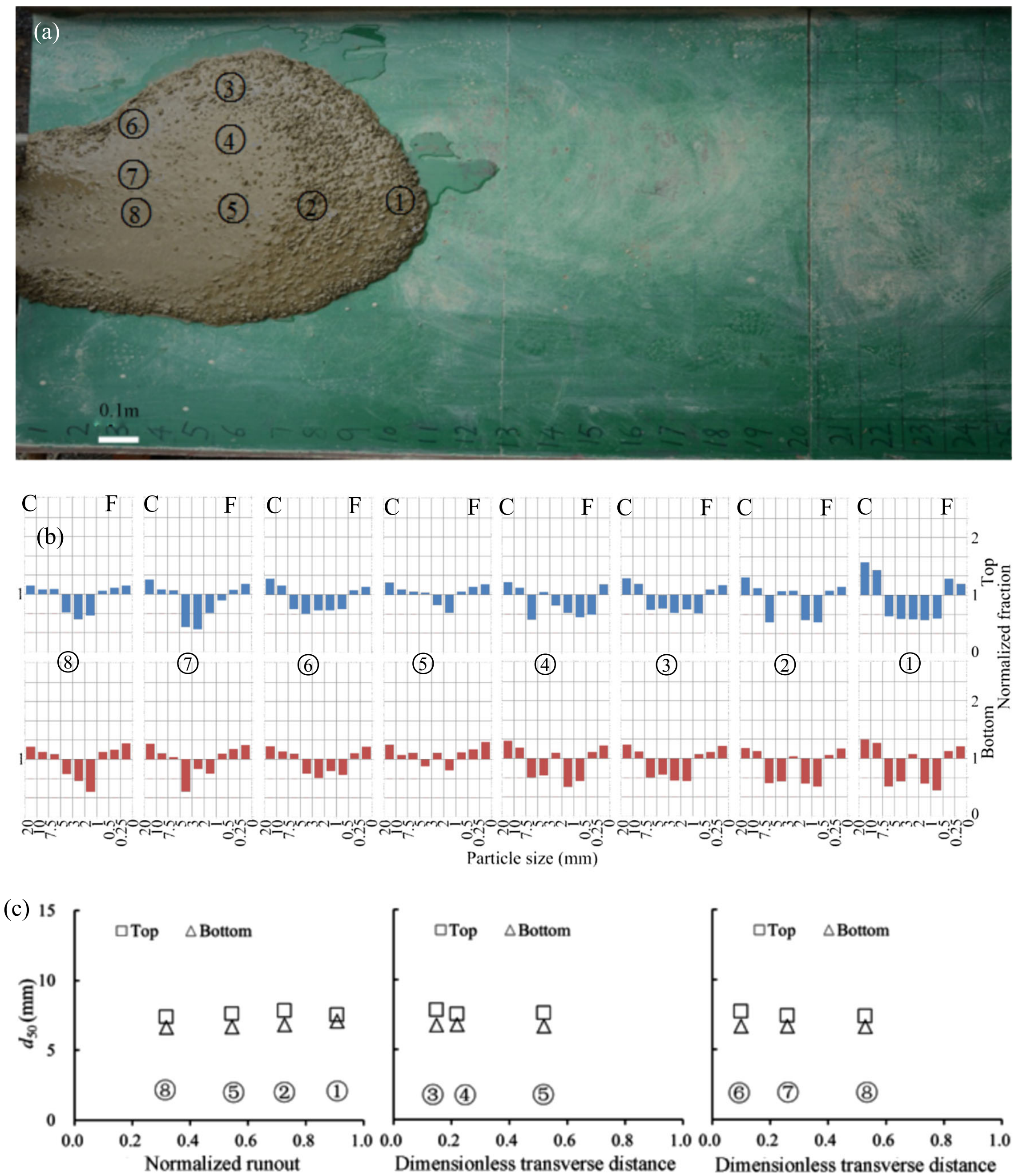

Fig. 17 Deposition and samples sites **a** in the fan of experimental debris flow with $w = 22.0\%$ ($C_s = 0.52$). **b** Relative abundance plots of deposit granulometry of samples. Coarse material (C) is to the left and fine material (F) to the right. Bars below the centerline indicate depletion and those above the centerline indicate enrichment. **c** The mean particle size (d_{50}) of each sample

22.0 to 32.5% results in an increase of the runout distance, deposition area, and deposited volume by about 3.0, 5.2, and 4.0 times, respectively. Similarly, higher water contents lead to a lower deposition heights and greater runout-width ratios because of lower shear resistance between grains.

Furthermore, the relationships among key dimensionless numbers (Bagnold number, Savage number, and Friction number) with the deposit area and the runout-width ratio are plotted in Fig. 11. Higher Bagnold and Savage numbers exhibit larger deposit areas and higher runout-width ratio. These findings suggest that inertial grain stress plays an integral role in the process of debris flow deposition. In other words, a positive relationship between the deposit area, runout-width ratio, and the inertial grain stresses exists. Distinct relationships between the deposit area, runout-width ratio, and the Friction number are unobvious.

Effects of flume slope

Debris flows passing over an abrupt change in topography can significantly alter flow kinematics and dynamics (Iverson et al. 2004; Sulpizio et al. 2008). Results in this study show that the morphology of the deposited sediment is strongly influenced by the inclination of the channel. For example, configuration I exhibits an elliptical morphology, while configuration II exhibits a strip-like morphology (Fig. 12). For similar debris flow mixtures, the runout distance and deposition area are greater for configuration II compared to that of configuration I, correspondingly, and the maximum deposit height is larger for configuration I.

The differences in morphology are a product of momentum transfer along the topography. The slope-dependent runout depends on momentum input from collision (vertical component) and slipping (horizontal component) processes. More specifically, the local curvature at the break between the inclined section and the outflow plane controls the separation of velocity into components that are perpendicular and parallel to the slope. These components govern the flow motion and velocity attenuation (Denlinger and Iverson 2001; Zhao et al. 2017). Although a steeper UC slope (45°) can increase gravitational potential energy, the abrupt change in slope to 0.0° (a flat DC slope) correspondingly increases the vertical momentum component. This leads to more intense collisions between the debris and the base of the channel, thereby decreasing the speed and runout distance. By contrast, a gentler UC slope (30°) in configuration II followed by a non-horizontal DC slope (7.6°) provides a smoother transition for the debris. Such a transition promotes a more efficient downstream motion which effectively increases runout distances. Beyond the break on the slope, the attenuation in flow velocity induces a deposition of debris and partial transfer of momentum into the generation of turbulence.

Effects of grain size distribution

The effects of GSD on the morphology of the deposited material were investigated in experiments (CI-GI-17.5 versus CI-GII-17.5, CI-GI-20.0 versus CI-GII-20.0, CI-GI-23.0 versus CI-GII-23.0, and CII-GII-28.5 versus CII-GI-28.5, Table 1).

Results show that an increase in fines content reduces the maximum runout distance (Fig. 13a1–a2 and b1–b2) because of the increased likelihood of grain-contact stresses, via collisions and enduring contacts, which dissipates flow kinetic energy.

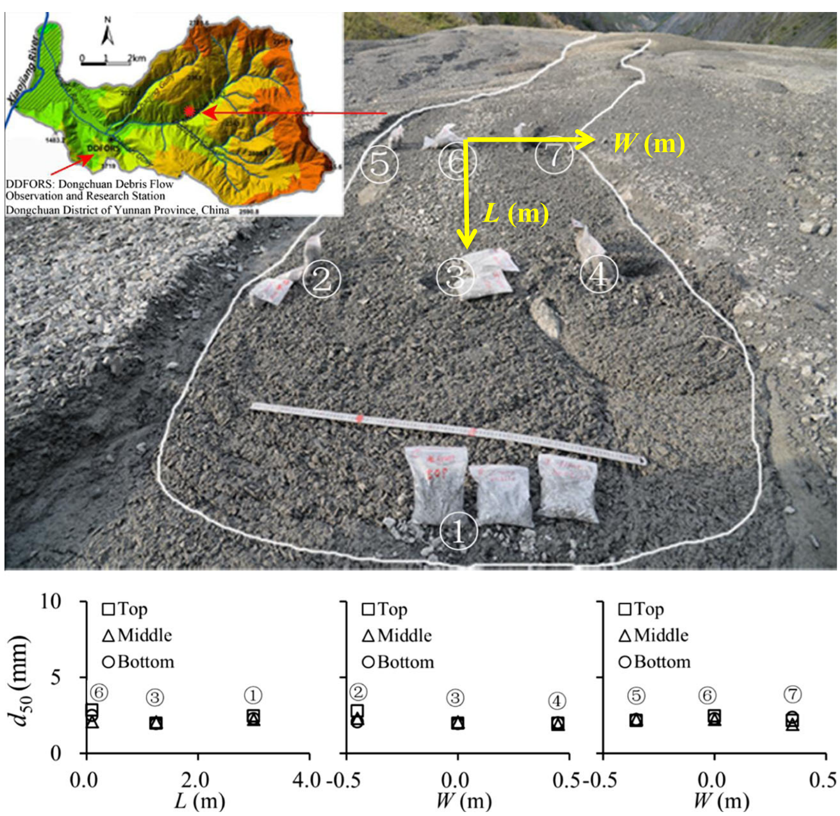

Fig. 18 Field sampling and analysis of the debris flows occurred in Jiangjia Gully (August 2017) by DDFORS

Additionally, the resistance-driven force ratio of a solid particle in the debris body flowing down along an inclined slope is dependent on $1/\delta$ (δ is the characteristic particle diameter, d_{50}), which governs flow mobility (Zhou et al. 2016). This implies that coarse particles should exhibit greater mobility. Nevertheless, the runout distance of GSDII becomes longer when water content equals to 28.5% (Fig. 13c1–c2). Such findings show water content more significantly governs the runout distance compared to fines content.

Grain size segregation

In order to highlight the evolution of the grain-size distributions that resulted from granular segregation, the deposit granulometric results against the granulometry of the initial solids mixture were normalized. There are two transverse transects, and each transect contains grains from three sample sites (Figs. 14a, 15a, 16a, and 17a). The central axial transect is comprised of four sample sites. At each sample site, a thin-walled steel shovel was inserted into the deposit body and the material within it was carefully excavated starting from the top and then to the bottom halves. To normalize a GSD, the proportion of dry mass in each size bin is divided by the corresponding proportion in the mean initial grain-size distribution. The histogram bars above the centerline in Figs. 14b, 15b, 16b, and 17b indicate enrichment (values > 1); otherwise, those bars below the centerline indicate depletion (values < 1) of material (Johnson et al. 2012).

Grain size segregation shows obvious differences among experimental sublets. When the water content is larger than 22.0%, segregation and accumulation of the coarse particles are less obvious from the flow front to the tail and from the lateral margin levees to the centerline (Figs. 14a, 15a, and 16a). More concretely, as shown in Figs. 14b, 15b, and 16b, the coarse particles are strongly enriched throughout the margin levees while the fines are correspondingly depleted (sample sites ③ and ⑥). Likewise, the center of the leveed channel (sample sites ⑤ and ⑧) exhibits an abundance of fines and a deficiency of coarse material. Lateral and distal margins of the deposited materials contain most coarse material (sample sites ①, ③, and ⑥) compared to the core of the deposition only a few tens of centimeters away (sample sites ⑤ and ⑧). When the water content is less than 22% or solid fraction higher than 0.52 (Fig. 17a), the deposited material exhibits a circular or ellipsoidal shape that is relatively homogenous and unsorted. Specifically in Fig. 17b, the sediments adjacent to lateral margin of deposits (sample sites ④ and ⑦) do not differ substantially from sediments further away from the margins (sample sites ⑤ and ⑧). This observation suggests that the particle sorting is strongly regulated by the fluid phase within debris flows. Results further corroborate that particle segregation can facilitate the development of the levee channel, which increase the runout distance (cf. Kokelaar et al. 2014).

Furthermore, the mean particle size (d_{50}) is used as the characteristic particle size in the analysis of the evolution of the sediment size distribution on debris flow fans. The d_{50} gradually increases from the tail to the front in the deposited material along the central axis (Figs. 14c, 15c, and 16c, sites ⑧, ⑤, ②, and ①) and from the center towards the edges in the transverse direction (sites ⑤, ④, and ③; ⑧, ⑦, and ⑥). This feature implies that the coarse particles accumulate at the flow front (levee), followed by a tail comprising a dilute mixture of fines (center). As for the distribution of particles with depth, the d_{50} of the top layer is substantially coarser than the d_{50} of the bottom layer. However, this phenomenon gradually becomes less obvious when the solid fraction is higher than 0.52 (Fig. 17c). This implied that grain-size segregation is inhibited in the viscous solid-rich experimental debris flow (solid fraction higher than 0.52). Neglecting shear rate effects, grain geometries, and physicochemical influences of Van der Waals or electrostatic forces between clay and colloidal particles, based on an empirical formula developed by Thomas (1965), predicts an increased effective Newtonian viscosity as a consequence of increased fines concentration in the fluid fraction and it provides a useful guideline (Iverson 1997):

$$\mu/\mu_w = 1 + 2.5\upsilon_{\text{fines}} + 10.05\upsilon_{\text{fines}}^2 + 0.00273\exp(16.6\upsilon_{\text{fines}}) \tag{7}$$

where μ_w is the dynamic viscosity of pure water (0.001002 Pa s) and υ_{fines} is the volume fraction of the interstitial fluid occupied by fines. Larger solid fraction C_s generally corresponds to larger values of υ_{fines}. Equation 7 shows the importance of pore fluid viscous shearing force ($(1 - C_s)(\gamma)\mu$) for is maintaining the suspension of solids and inhibiting the pertinent segregation induced by solid contacts (collision and contact friction). It would be apparent that the role of viscosities in these debris flows cannot be downplayed in the deposition process.

To further verify the experimental results, field sampling at a natural debris flow deposition area from the Menqian Gully (a tributary upstream of Jiangjia Gully) was carried out after a debris flow event. The density of the debris material was measured as 2194 kg/m^3, which corresponds to a water content of 46.0% and solid fraction of 0.54.

The mean particle size d_{50} at different positions throughout the deposit area was measured by using sieve analyses (Fig. 18). Results showed that the mean particle sizes were almost equal, indicating that particle sorting is not obvious for highly viscous debris flow, which is consistent with the flume test results in this study.

Conclusions

This study provides an improved understanding of the deposition process and the prevailing morphology of the deposited debris. More specifically, the effects of water content, grain size distribution of the debris flow mixture, and channel configuration are examined. Key findings can be drawn as follows:

1. The presented experimental debris flows fall into either viscous ($N_{\text{Bag}} < 200$) or collisional ($N_{\text{Sav}} > 0.1$) flow regimes, similar to those occurred in the nature. Both the deposition area and runout-to-width ratio increase with inertial grain stresses due to collisions ($\delta^2\dot{\gamma}^2$), manifested in the particle size (δ) and shear rate ($\dot{\gamma}$) of the debris mixture.
2. Most experimental debris flow fronts lack sustained pore fluid pressures. Such pressures are important in regulating grain-grain and grain-bed friction and collisions during the deposition process. The measured excess pore fluid pressure (positive) in the granular body is beneficial for debris flow mobility.
3. The water content and fines content of a debris flow have profound effects on deposition morphology. Debris flows with high water content flows are longer and thinner than those of low water content. Runout distance and deposition area increase with water contents. Furthermore, an increase in fines content can reduce the runout distance due to the enhanced

solids contact energy dissipation. However, this effect is limited when the water content of debris flow is high (e.g., w = 28.5% in this study).

4. The topography where the debris flow transfers from transportation to the deposition process significantly alters the flow dynamics and strongly influences the runout distance and deposition morphology. A smoother transition between a steep sections followed by a gentler section promotes a more efficient downstream motion which effectively increases the runout distance.
5. When the solid fraction of debris flows is less than 0.52, the mean particle size of the deposited material gradually increased from the tail to the front, towards the edges of the flow, and vertically towards the free surface. For debris flows with high solid fraction ($C_s > 0.52$ in this study), pore fluid viscous shearing force (for the maintaining of solids well suspended in the mixtures) plays an important role in reducing the segregation of solids. Particle sorting is not obvious on the deposit fan.

Funding The authors acknowledge the financial support from the National Natural Science Foundation of China (Grant Nos. 11672318, 41731283), the Youth Innovation Promotion Association, Chinese Academy of Sciences (CAS), the CAS "Light of West China" Program (Grant No. Y6R2220220), the CAS Pioneer Hundred Talents Program, and the Research Grants Council of the Government of Hong Kong SAR, China (Grant T22-603/15-N).

Abbreviations

C_s	Volumetric solid fraction
d_{50}	Mean particle size
Fr	Froude number
h	Approaching flow depth
g	Gravitational acceleration
N_{Bag}	Bagnold number
N_{Sav}	Savage number
N_{Fric}	Friction number
p_{bed}	Pore pressure
σ_{bed}	Normal stress
v	Debris flow velocity
w	Water content
ρ_f	Density of the fluid
ρ_s	Density of the solids
μ	Interstitial fluid viscosity
μ_w	Dynamic viscosity of pure water
$\upsilon_{\mathrm{fines}}$	Volume fraction of the interstitial fluid occupied by fines
ϕ	Friction angle between grains
$\gamma^{\cdot}$	Shear rate
θ	Channel inclination
δ	Characteristic size of the sediments
Δu	Excessive pore fluid pressure

References

Berti M, Genevois R, Simoni A, Tecca PR (1999) Field observations of a debris flow event in the Dolomites. Geomorphology 29:256–274

Berti M, Genevois R, LaHusen A, Simoni TPR (2000) Debris flow monitoring in the acquabona watershed on the Dolomites (Italian alps). Phys Chem Earth (B) 25(9):707–715

Chen X, Cui Y (2017) The formation of the Wulipo landslide and the resulting debris flow in Dujiangyan City, China. J Mt Sci 14(6):1100–1112

Choi CE, Ng CWW, Au-Yeung SCH, Goodwin G (2015) Froude scaling of landslide debris in flume modelling. Landslides 12(6):1197–1206

Cui P, Chen X, Wang Y, Hu K, Li Y (2005) Jiangjia Ravine debris flows in south-western China. In: Debris-flow hazards and related phenomena. Berlin: Springer, pp 565–594

Cui P, Zhou GGD, Zhu XH, Zhang JQ (2013) Scale amplification of natural debris flows caused by cascading landslide dam failures. Geomorphology 182:73–189

Cui Y, Zhou X, Guo C (2017) Experimental study on the moving characteristics of fine grains in wide grading unconsolidated soil under heavy rainfall. J Mt Sci 14(3):417–431

Cui Y, Choi CE, Liu LHD, Ng CWW (2018) Effects of particle size of monodispersed granular flows impacting a rigid barrier. Nat Hazards 91(3):1179–1201

D'Agostino V, Cesca M, Marchi L (2010) Field and laboratory investigations of runout distances of debris flows in the Dolomites (Eastern Italian Alps). Geomorphology 115(3):94–304

D'Agostino V, Bettella F, Cesca M (2013) Basal shear stress of debris flow in the runout phase. Geomorphology 201:272–280

Davies TRH (1990) Debris-flow surges: experimental simulation. J Hydrol N Z 29(1):18–46

Denlinger RP, Iverson RM (2001) Flow of variably fluidized granular masses across three dimensional terrain: II. Numerical predictions and experimental tests. J Geophys Res Solid Earth 106:553–566

Dufresne A (2012) Granular flow experiments on the interaction with stationary runout path materials and comparison to rock avalanche events. Earth Surf Process Landf 37(14):1527–1541

Faug T (2015) Macroscopic force experienced by extended objects in granular flows over a very broad Froude-number range. Eur Phys J E 38(5):13–16

Haas T, Braat L, Leuven JR, Lokhorst IR, Kleinhans MG (2015) Effects of debris flow composition on runout, depositional mechanisms, and deposit morphology in laboratory experiments. J Geophys Res Earth Surf 120:1949–1972

Hoblitt RP (1986) Observations of the eruptions of July 22 and August 7, 1980, at Mount St. Helens, Washington. US Geological Survey Professional Paper 1335, 44

Hsu KJ (1975) Catastrophic debris streams (sturzstroms) generated by rockfalls. Geol Soc Am Bull 86:129–140

Hsu KJ (1978) Albert Hiem: observations on landslides and relevance to modern interpretations. In: Voight B (ed) Rockslides and avalanches: natural phenomena. Elsevier, Amsterdam, pp 71–93

Hsu L, Dietrich WE, Sklar LS (2008) Experimental study of bedrock erosion by granular flows. J Geophys Res Earth Surf 113:F02001

Hübl J, Suda J, Proske D (2009) Debris flow impact estimation. In: The 11th international symposium on water management and hydraulic Eng Conf Ohrid, Macedonia, pp 1–4

Hürlimann M, Rickenmann D, Graf C (2003) Field and monitoring data of debris-flow events in the Swiss Alps. Can Geotech J 40(1):161–175

Hürlimann M, McArdell BW, Rickli C (2015) Field and laboratory analysis of the runout characteristics of hillslope debris flows in Switzerland. Geomorphology 232:20–32

Iverson RM (1997) The physics of debris flows. Rev Geophys 35(3):245–296

Iverson RM (2015) Scaling and design of landslide and debris-flow experiments. Geomorphology 244:9–20

Iverson RM, Denlinger RP (2001) Flow of variably fluidized granular masses across three-dimensional terrain: 1. Coulomb mixture theory. J Geophys Res Solid Earth 106(B1):537–552

Iverson RM, Vallance JW (2001) New views of granular mass flows. Geology 29(2):115–118

Iverson RM, Logan M, Denlinger RP (2004) Granular avalanches across irregular three-dimensional terrain: 2. Experimental tests. J Geophys Res Earth Surf 109:F01015

Iverson RM, Logan M, LaHusen RG, Berti M (2010) The perfect debris flow? Aggregated results from 28 large-scale experiments. J Geophys Res Earth Surf 115:F03005

Johnson C, Kokelaar B, Iverson RM, Logan R, LaHusen, Gray J (2012) Grain-size segregation and levee formation in geophysical mass flows. J Geophys Res Earth Surf 117:F01032

Kim Y, Paik J (2015) Depositional characteristics of debris flows in a rectangular channel with an abrupt change in slope. J Hydro Environ Res 9(3):420–428

Kokelaar BP, Graham RL, Gray J, Vallance JW (2014) Fine-grained linings of leveed channels facilitate runout of granular flows. Earth Planet Sci Lett 385:172–180

Kuntz MA, Rowley PD, MacLeod NS, Reynolds RL, McBroome LA, Kaplan AM, Lidke DJ (1981) Petrography and particle size distribution of pyroclastic-flow, ash-cloud, and surge deposits, US Geological Survey Professional Paper 1250: 525–539

Li Y, Liu J, Su F, Xie J, Wang B (2015) Relationship between grain composition and debris flow characteristics: a case study of the Jiangjia Gully in China. Landslides 12(1):19–28
Major JJ (1997) Depositional processes in large-scale debris-flow experiments. J Geol 105(3):345–366
Major JJ, Iverson RM (1999) Debris-flow deposition: effects of pore-fluid pressure and friction concentrated at flow margins. Geol Soc Am Bull 111(10):1424–1434
McArdell BW, Bartelt P, Kowalski J (2007) Field observations of basal forces and fluid pore pressure in a debris flow. Geophys Res Lett 34:L07406
Parsons JD, Whipple KX, Simoni A (2001) Experimental study of the grain-flow, fluid-mud transition in debris flows. J Geol 109(4):427–447
Scheidl C, Rickenmann D (2010) Empirical prediction of debris-flow mobility and deposition on fans. Earth Surf Process Landf 35(2):157–173
Scheidl C, Rickenmann D, McArdell BW (2013) Runout prediction of debris flows and similar massmovements. In: Landslide science and practice. Springer, Berlin,pp 221–229
Shu AP, Tang C, Zhang X, Shao SD, Yang K (2015) Deposition morphology of non-homogeneous debris flow and its energy characteristics. J Mt Sci 12(5):1157–1168
Stancanelli LM, Lanzoni S, Foti E (2015) Propagation and deposition of stony debris flows at channel confluences. Water Resour Res 51:5100–5116
Sulpizio R, De Rosa R, Donato P (2008) The influence of variable topography on the depositional behaviour of pyroclastic density currents: the examples of the Upper Pollara eruption (Salina Island, southern Italy). J Volcanol Geotherm Res 175:367–385
Sun H, Lam T, Tsui H (2005) Design basis for standardized modules of landslide debris-resisting barriers. GEO Report No. 174, Geotech Eng Office, Civ Eng Department, The Government of Hong Kong Special Administrative Region
Takahashi T (1991) Debris flow. Balkema, Rotterdam
Tang C, Zhu J, Chang M, Ding J, Qi X (2012) An empirical–statistical model for predicting debris-flow runout zones in the Wenchuan earthquake area. Quat Int 250:63–73
Thomas DG (1965) Transport characteristics of suspension: VIII. A note on the viscosity of Newtonian suspensions of uniform spherical particles. J Colloid Sci 20(3):267–277
Van Steun H, Coutard JP (1989) Laboratory experiments with small debris flows: physical properties related to sedimentary characteristics. Earth Surf Process Landf 14(6):587–596
Wilson L, Head JW (1981) Morphology and rheology of pyroclastic flows and their deposits, and guidelines for future observations, US Geological Survey Professional Paper 1250: 513–524
Zhao T, Crosta GB, Utili S, De Blasio FV (2017) Investigation of rock fragmentation during rockfalls and rock avalanches via 3-D discrete element analyses. J Geophys Res Earth Surf 122(3):678–695
Zhou GGD, Ng CWW (2010) Dimensional analysis of natural debris flows. Can Geotech J 47(7):719–729
Zhou GGD, Wright NG, Sun Q, Cai Q (2016) Experimental study on the mobility of channelized granular mass flow. Acta Geol Sin 90(3):988–998
Zhou GGD, Song D, Choi CE, Pasuto A, Sun QC, Dai DF (2018) Surge impact behavior of granular flows: effects of water content. Landslides 15(4):695–709

G. G. D. Zhou · S. Li (✉) · D. Song · X. Chen
Key Laboratory of Mountain Hazards and Earth Surface Process/Institute of Mountain Hazards and Environment,
Chinese Academy of Sciences (CAS),
Chengdu, China
Email: lishuai@imde.ac.cn

G. G. D. Zhou
e-mail: gordon@imde.ac.cn

D. Song
e-mail: drsong@imde.ac.cn

X. Chen
e-mail: xqchen@imde.ac.cn

G. G. D. Zhou · S. Li · D. Song · X. Chen
University of Chinese Academy of Sciences,
Beijing, China

C. E. Choi
Department of Civil and Environmental Engineering,
The Hong Kong University of Science and Technology, HKSAR,
Hong Kong, China
e-mail: ceclarence@ust.hk

C. E. Choi
The HKUST Jockey Club Institute for Advanced Study, HKSAR,
Hong Kong, China

C. E. Choi
HKUST Fok Ying Tung Graduate School,
Nansha, Guangzhou, China